

Generation and detection of broadband multi-channel orbital angular momentum by micrometer-scale meta-reflectarray

Jinpeng Liu,¹ Changjun Min,^{2,4} Ting Lei,² Luping Du,² Yangsheng Yuan,^{2,3} Shibiao Wei,² Yiping Wang,² and X.-C. Yuan^{2,5}

¹*Institute of Modern Optics, Nankai University, Tianjin 300071, China*

²*Nanophotonics Research Centre, Shenzhen University & Key Laboratory of Optoelectronic Devices and Systems of Ministry of Education and Guangdong Province, College of Optoelectronic Engineering, Shenzhen University, 518060, China*

³*Department of Physics, Anhui Normal University, Wuhu 241000, China*

⁴*cjmin@szu.edu.cn*

⁵*xcyuan@szu.edu.cn*

Abstract: We theoretically demonstrate the generation and detection of broadband multi-channel Orbital Angular Momentum(OAM) by a micrometer-scale meta-reflectarray. The meta-reflectarray composed of patterned silicon bars on a silver ground plane can be designed to realize phase modulation and work as chip-level OAM devices. Compared to traditional methods of OAM generation and detection, our approach shows superiorities of very compact structure size, broadband working wavelength (1250-1750nm), high diffraction efficiency (~70%), simultaneously handling multiplex OAMs, and tunable reflection angle (0-45°). These fascinating advantages provides great potential applications in photonic integrated devices and systems for high-capacity and multi-channel OAM communication.

©2016 Optical Society of America

OCIS codes: (050.4865) Optical vortices; (060.4510) Optical communications; (230.3990) Micro-optical devices.

References and links

1. J. F. Nye and M. V. Berry, "Dislocations in wave trains," *Proc. R. Soc. Lond. A Math. Phys. Sci.* **336**(1605), 165–190 (1974).
2. P. Couillet, L. Gil, and F. Rocca, "Optical vortices," *Opt. Commun.* **73**(5), 403–408 (1989).
3. J. E. Curtis and D. G. Grier, "Structure of optical vortices," *Phys. Rev. Lett.* **90**(13), 133901 (2003).
4. L. Allen, M. W. Beijersbergen, R. J. C. Spreeuw, and J. P. Woerdman, "Orbital angular momentum of light and the transformation of Laguerre-Gaussian laser modes," *Phys. Rev. A* **45**(11), 8185–8189 (1992).
5. L. Allen, S. M. Barnett, and M. J. Padgett, *Orbital Angular Momentum* (Institute of Physics Publishing, 2003).
6. J. Wang, J. Y. Yang, I. M. Fazal, N. Ahmed, Y. Yan, H. Huang, Y. X. Ren, Y. Yue, S. Dolinar, M. Tur, and A. E. Willner, "Terabit free-space data transmission employing orbital angular momentum multiplexing," *Nat. Photonics* **6**(7), 488–496 (2012).
7. X. Cai, J. Wang, M. J. Strain, B. Johnson-Morris, J. Zhu, M. Sorel, J. L. O'Brien, M. G. Thompson, and S. Yu, "Integrated compact optical vortex beam emitters," *Science* **338**(6105), 363–366 (2012).
8. T. Lei, M. Zhang, Y. Li, P. Jia, G. N. Liu, X. Xu, Z. Li, C. Min, J. Lin, C. Yu, H. Niu, and X. C. Yuan, "Massive individual orbital angular momentum channels for multiplexing enabled by Dammann gratings," *Light Sci. Appl.* **4**(3), e257 (2015).
9. M. J. Strain, X. Cai, J. Wang, J. Zhu, D. B. Phillips, L. Chen, M. Lopez-Garcia, J. L. O'Brien, M. G. Thompson, M. Sorel, and S. Yu, "Fast electrical switching of orbital angular momentum modes using ultra-compact integrated vortex emitters," *Nat. Commun.* **5**, 4856 (2014).
10. S. Yu, "Potentials and challenges of using orbital angular momentum communications in optical interconnects," *Opt. Express* **23**(3), 3075–3087 (2015).
11. N. Zhang, J. A. Davis, I. Moreno, D. M. Cottrell, and X. C. Yuan, "Analysis of multilevel spiral phase plates using a Dammann vortex sensing grating," *Opt. Express* **18**(25), 25987–25992 (2010).
12. N. Zhang, X. C. Yuan, and R. E. Burge, "Extending the detection range of optical vortices by Dammann vortex gratings," *Opt. Lett.* **35**(20), 3495–3497 (2010).

13. X. L. Cai, Y. J. Chen, and S. Y. Yu, "Integrated photonic orbital angular momentum devices and systems: Potentials and challenges," *Sci. China B* **56**(3), 579–585 (2013).
14. N. Yu, P. Genevet, M. A. Kats, F. Aieta, J. P. Tetienne, F. Capasso, and Z. Gaburro, "Light propagation with phase discontinuities: Generalized laws of reflection and refraction," *Science* **334**(6054), 333–337 (2011).
15. C. L. Holloway, E. F. Kuester, J. A. Gordon, J. O'Hara, J. Booth, and D. R. Smith, "An overview of the theory and applications of metasurfaces: The two dimensional equivalents of metamaterials," *IEEE Antennas Propag. Mag.* **54**(2), 10–35 (2012).
16. A. V. Kildishev, A. Boltasseva, and V. M. Shalaev, "Planar photonics with metasurfaces," *Science* **339**(6125), 1232009 (2013).
17. N. Yu and F. Capasso, "Flat optics with designer metasurfaces," *Nat. Mater.* **13**(2), 139–150 (2014).
18. F. Aieta, A. Kabiri, P. Genevet, N. Yu, M. A. Kats, Z. Gaburro, and F. Capasso, "Reflection and refraction of light from metasurfaces with phase discontinuities," *J. Nanophotonics* **6**(1), 063532 (2012).
19. F. Aieta, P. Genevet, M. A. Kats, N. Yu, R. Blanchard, Z. Gaburro, and F. Capasso, "Aberration-free ultrathin flat lenses and axicons at telecom wavelengths based on plasmonic metasurfaces," *Nano Lett.* **12**(9), 4932–4936 (2012).
20. N. Yu, F. Aieta, P. Genevet, M. A. Kats, Z. Gaburro, and F. Capasso, "A broadband, background-free quarter-wave plate based on plasmonic metasurfaces," *Nano Lett.* **12**(12), 6328–6333 (2012).
21. X. Yin, Z. Ye, J. Rho, Y. Wang, and X. Zhang, "Photonic spin Hall effect at metasurfaces," *Science* **339**(6126), 1405–1407 (2013).
22. L. Huang, X. Chen, H. Mühlenbernd, G. Li, B. Bai, Q. Tan, G. Jin, T. Zentgraf, and S. Zhang, "Dispersionless phase discontinuities for controlling light propagation," *Nano Lett.* **12**(11), 5750–5755 (2012).
23. E. Karimi, S. A. Schulz, I. De Leon, H. Qassim, J. Upham, and R. W. Boyd, "Generating optical orbital angular momentum at visible wavelengths using a plasmonic metasurface," *Light Sci. Appl.* **3**(5), e167 (2014).
24. Y. Yang, W. Wang, P. Moitra, I. I. Kravchenko, D. P. Briggs, and J. Valentine, "Dielectric meta-reflectarray for broadband linear polarization conversion and optical vortex generation," *Nano Lett.* **14**(3), 1394–1399 (2014).
25. K. E. Chong, I. Staude, A. James, J. Dominguez, S. Liu, S. Campione, G. S. Subramania, T. S. Luk, M. Decker, D. N. Neshev, I. Brener, and Y. S. Kivshar, "Polarization-independent silicon metadevices for efficient optical wavefront control," *Nano Lett.* **15**(8), 5369–5374 (2015).
26. M. I. Shalaev, J. Sun, A. Tsukernik, A. Pandey, K. Nikolskiy, and N. M. Litchinitser, "High-efficiency all-dielectric metasurfaces for ultracompact beam manipulation in transmission mode," *Nano Lett.* **15**(9), 6261–6266 (2015).
27. S. Sun, K. Y. Yang, C. M. Wang, T. K. Juan, W. T. Chen, C. Y. Liao, Q. He, S. Xiao, W. T. Kung, G. Y. Guo, L. Zhou, and D. P. Tsai, "High-efficiency broadband anomalous reflection by gradient meta-surfaces," *Nano Lett.* **12**(12), 6223–6229 (2012).
28. L. Huang, X. Chen, H. Mühlenbernd, H. Zhang, S. Chen, B. Bai, Q. Tan, G. Jin, K. Cheah, C. Qiu, J. Li, T. Zentgraf, and S. Zhang, "Three-dimensional optical holography using a plasmonic metasurface," *Nat. Commun.* **4**, 2808 (2013).
29. M. W. Beijersbergen, R. Coerwinkel, M. Kristensen, and J. P. Woerdman, "Helical-wavefront laser beams produced with a spiral phase plate," *Opt. Commun.* **112**(5–6), 321–327 (1994).
30. N. R. Heckenberg, R. McDuff, C. P. Smith, and A. G. White, "Generation of optical phase singularities by computer-generated holograms," *Opt. Lett.* **17**(3), 221–223 (1992).
31. G. Zheng, H. Mühlenbernd, M. Kenney, G. Li, T. Zentgraf, and S. Zhang, "Metasurface holograms reaching 80% efficiency," *Nat. Nanotechnol.* **10**(4), 308–312 (2015).

1. Introduction

Optical vortex (OV) is a special light with spiral phase distribution around its travel axis and a phase singularity for the uncertainty of phase in the center [1–3]. Its spiral phase factor $\exp(i\theta)$, l for topological charge and θ for azimuth angle, makes each photon have the orbital angular momentum (OAM) of $l\hbar$ [4,5]. Theoretically, as the value of l increases, the OAM of photon has infinite value. Consequently, as a new degree of freedom for information encoding and decoding, OAM has been proved to have significant potential in free-space optical communication system to realize high-capacity and multi-channel communications [6–10]. The practical applications of OAM will probably require photonic integrated devices and circuits for miniaturization, improved performance, and enhanced functionality. However, most traditional methods of OAM's generation and detection are based on large-sized optical devices such as spatial light modulator and fork gratings [11,12], which are only suitable for large communication systems rather than the integrated lab-on-chip systems. Therefore, to address this problem, the research of chip-level OAM's generation and detection device has become a hotspot [8,13].

As a candidate of chip-scale OAM devices, recently, a type of tiny and ultrathin interfaces called “metasurface” has been presented [14–17]. The metasurface consisting of specially designed patterns of nano-antennas, can realize modulations on optical phase and amplitude over a broad wavelength range. Such properties of metasurface make it a very valuable micrometer-scale device in many novel optical applications, such as anomalous refraction and reflection [18], aberration-free lenses and axicons [19], micrometer-scale quarter wavelength plate [20], photonic spin hall effect [21], and optical vortex generations [22–26].

In this letter, for the first time, we introduce metasurface to OAM communication field. The OAM communication requires generating and detecting a large number of OV’s for multiplexing [6, 8], but most previous studies of metasurfaces only showed the generation of a single OV [22–26], not designed for practical applications of OAM communication. Thus, here we first design the metasurface-based OAM devices for communication applications, and investigate the generation and detection for multiple OV’s with different OAMs by finite difference time domain (FDTD) method. Our designs are based on a type of metasurface called “meta-reflectarray” [24], which consists of patterned silicon bars attached on a PMMA layer over a silver film to realize phase modulation on the reflected beam. Instead of using large-size polarization filter to filter out useless reflected light [24], we design a gradient phase in our meta-reflectarray, which make the signal light output in a tunable reflection angle and keep the device in micrometer size. Such meta-reflectarray benefits from the low-loss dielectric nano-antennas, thereby achieving higher efficiency than many other metasurfaces composed of metallic nano-antennas [18–22]. Through studying the reflectance spectrum of designed meta-reflectarray, we reveal that such generated OV array has a maximum diffraction efficiency of $\sim 70\%$ and a broad bandwidth from 1250nm to 1750nm (covers the communication wavelengths of 1310nm and 1550nm). Finally, besides multi-OAM’s generation, we also demonstrate the valuable capability of multi-OAM’s detection in our meta-reflectarray. Compared to traditional methods of multi-OAM’s generation and detection, our approach has various advantages, including the very compact structure size for integrated devices, generation and detection for multiplex OAMs, high diffraction efficiency, broadband working wavelength, and tunable reflection angle. Thus, our research has great potential applications for chip-level high-efficiency high-capacity OAM communication and modulation devices.

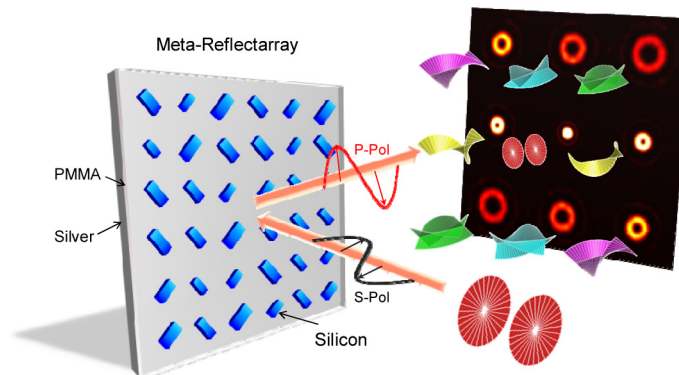


Fig. 1. Schematic of a 3×3 OV array generated by a meta-reflectarray. The meta-reflectarray contains 8 kinds of Si-bars providing an incremental phase shift of $\pi/4$ [24], including four sizes (length $l = 425\text{nm}$, width $w = 200\text{nm}$; $l = 435\text{nm}$, $w = 225\text{nm}$; $l = 450\text{nm}$, $w = 250\text{nm}$; $l = 475\text{nm}$, $w = 275\text{nm}$) and two inclined ± 45 degree by horizontal direction. The thickness and permittivity of silicon, PMMA, silver layers are 380nm, 200nm, 800nm and 12.376, 2.25, $86.642 + 4.371i$ (at 1550nm), respectively. The incident light is an *s*-polarized Gauss beam with a wavelength range from 1250nm to 1750nm, and the reflected OV array is *p*-polarized. The size of whole meta-reflectarray is about $40 \times 40\mu\text{m}^2$, containing 60×60 Si-bars with period size $650 \times 650\text{nm}^2$.

2. Generation of OAM array

In Fig. 1, we show a schematic of generating a 3×3 OV array by meta-reflectarray. The meta-reflectarray is a designed pattern of silicon-bars attached on a PMMA layer over a silver film. Here the single Si-bar can be considered as a dielectric resonator, and its resonance generates a phase shift to reflected beam from 0 to 2π depending on its size and orientation [24]. Thus we can design an accurate distribution of Si-bars with different sizes and orientations to get the desired phase distribution, such as spiral phase for generating single OV or complex vortex gratings for generating OV arrays [11].

As shown in Fig. 1, when an s -polarized Gaussian beam is vertically incident onto the meta-reflectarray, a part of incident light coupled to the resonance of Si-bars is modulated in phase and converted to orthogonal p -polarization (denoted as cross-polarization) due to the resonance, and then reflected to form the designed 3×3 OV array; while the other part is directly reflected without phase modulation and keeps the s -polarization (denoted as co-polarization). Since only the cross-polarized part carries the useful modulated phase, it is important to suppress the co-polarized part which is considered as useless background light and may disorder the generated OV array. In previous reports [24, 27, 28], researchers used a polarization filter to filter out the co-polarized reflected light, however, the large-size filter device is unsuitable for chip-scale communication systems. To solve this problem, here we add a gradient phase to the meta-reflectarray (Fig. 2(a)) and realize tilt reflection of the cross-polarized light just like a blazed grating, while the co-polarized part remains normal reflection, therefore the co- and cross-polarized parts are separated in different reflection angles.

The phase hologram of meta-reflectarray for generating 3×3 OV array is shown in Fig. 2(a), and the corresponding Si-bar distributions at central part are presented in Fig. 2(b). Through designing different phase holograms, we can generate OV array with arbitrary amount and OAM distribution. In Figs. 2(c)-2(e), we show examples of generated 3×3 , 4×4 and 5×5 OV arrays at 1550nm wavelength with different OAMs. The reflection angle for all OV array is chosen as 16.5 degree (optimized for better OV pattern) due to the gradient phase.

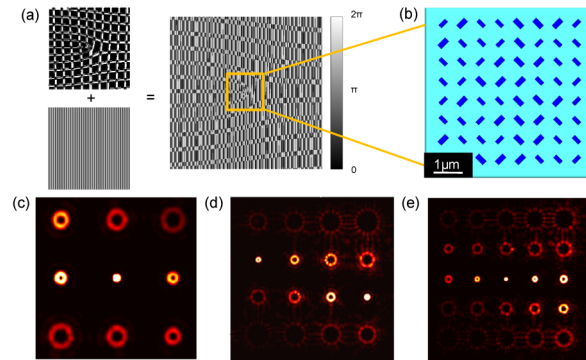


Fig. 2. Different amounts of OV array generated by meta-reflectarray. (a) Phase hologram of meta-reflectarray combined by a 2-dimensional Dammann vortex grating for generating 3×3 OV array and a gradient phase for tilt reflection. (b) Central part of meta-reflectarray in (a), including Si-bars (blue rectangles) and PMMA layer (light blue background). (c) - (e) are generated 3×3 , 4×4 , 5×5 OV arrays at 1550nm wavelength with corresponding topological charges $l = -4 \sim -4$, $-8 \sim -8$ and $-12 \sim -12$, respectively. The reflection angle of center point of all OV arrays is 16.5 degree.

3. Broadband and tunable reflection angle of meta-reflectarray

Conventional OAM's generation and detection devices based on dielectric gratings or spiral phase plate are usually suitable for a single wavelength [29,30], while the meta-reflectarray studied here has a valuable broadband response for a wide range around communication

wavelength (1550nm). To demonstrate such an advantage, we show the OAM array pattern generated in different wavelengths and the corresponding reflectance spectra of the meta-reflectarray in Fig. 3. Figure 3(a) presents the cross-polarized 3×3 OV array in the wavelength of 1250nm, 1500nm, 1600nm and 1750nm, respectively, using different colors for visualizing the different wavelengths. These results verify that the meta-reflectarray has the ability of generating OV array in a wide range of ~ 500 nm in wavelength. Such broadband response is due to the fact that each Si-bar has isolated resonant modes along long and short axis [24], and combination of these resonant modes in a periodic structure broadens the resonant response in spectrum. It is also observed that the generated OV array between 1500 and 1600nm are better than other wavelength, because the structure parameters of Si-bars in meta-reflectarray are mainly optimized for the communication wavelength of 1550nm.

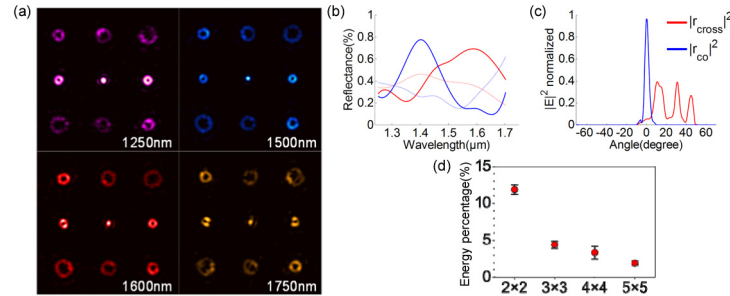


Fig. 3. (a) 3×3 OV array patterns obtained in the wavelength of 1250nm, 1500nm, 1600nm and 1750nm, respectively. (b) Reflectance as a function of incident wavelength range from 1250 to 1700nm. The solid lines are for normal reflection and dotted lines for tilt reflection of both co- (blue) and cross- (red) polarizations. (c) Far-field OV array intensity distribution as a function of reflection angle for both co- and cross-polarizations. (d) Uniformity of 2×2 – 5×5 OV arrays generated by meta-reflectarray. Energy percentage means the ratio of each OV's energy to the total incident energy.

The reflection spectra of the meta-reflectarray are shown in Fig. 3(b), where the red and blue curves represent the cross and co-polarized components. The reflection coefficient of co- and cross-polarized components of reflected beam is defined as r_{co} and r_{cross} , respectively, thus the corresponding normalized reflectance is $|r_{co}|^2$ and $|r_{cross}|^2$, respectively. We calculated the reflectance for both normal reflection (without gradient phase) as solid curves and tilt reflection (with gradient phase) as dotted curves. For the normal reflection, the diffraction efficiency (defined as ratio of the energy of reflected OV array to the total incident energy) of cross-polarized 3×3 OV array could reach almost 70% around 1600nm and maintain a broad peak, while the co-polarized part is strongly suppressed in that region. It is noted that here the nonuniform distribution of Si-bars with different sizes and orientations generates complex resonant modes with lots of useless scattering, and thus causes lower diffraction efficiency than the case of uniform Si-bars distribution with same resonant mode reported in [24]. For the tilt reflection, we add a gradient phase in the meta-reflectarray to get a tunable reflection angle from 0 to 45 degree for the cross-polarized OV array, in order to separate the co- and cross-polarized parts of reflected beam. The diffraction efficiency of the tilt reflection case still maintains a broad peak, but is lower than that of normal reflection, due to the fact that the gradient phase makes the resonant mode of whole structure more complicated, and thus induces more useless scattering. The intensity distribution as a function of reflection angle for the tilt reflection case is shown in Fig. 3(c). We can see that there are three peaks in the cross-polarized part at the angles of 10, 30 and 45 degree, respectively, in accordance with the three rows of 3×3 OV array. For the co-polarized reflected beam, the designed meta-reflectarray has no modulation effect and only serves as a mirror, hence the peak of co-polarized part only

appears at 0 degree. As a result, we achieve the separation of orthogonal polarizations without additional large-size optical polarization filter devices.

Based on the General Snell's law [14]: $n_i \sin \theta_i - n_t \sin \theta_t = \lambda/T$, we can control the reflection angle based on the phase abrupt of metasurface. T is the space length corresponding to phase change from 0 to 2π in gradient phase, here presenting as a length of several periods which induces phase change from 0 to 2π . θ_i and θ_t are incident angle and reflection angle, while n_i and n_t are the refractive indices of the two media: PMMA and air, respectively. λ is the free-space wavelength. In our calculation model, incident angle is 0, $n_t = 1$, thus we can simplify the equation as: $\sin \theta_t = \lambda/T$. Consequently, at a fixed wavelength, we can change T to turn the reflection angle θ_t at a range from 0 to 45 degree in 1550nm, and such method is also suitable for other wavelengths. Finally, to validate the uniformity of each OV's energy at different topological charges, averaged energy percentage of each OV with standard deviation for 2×2 , 3×3 , 4×4 and 5×5 OV arrays generated by designed meta-reflectarray are calculated and shown in Fig. 3(d), which presents little deviation and good uniformity for all OV arrays.

4. Detection of OAMs

Besides generating OV array, meta-reflectarray can also be used to detect multiple OVs with different OAMs. The schematic of OAM detection is basically same as the generation setup shown in Fig. 1, except replacing the incident Gauss beam to single or multiple coaxial OVs as incident beam. When an OV with topological charge l is incident onto meta-reflectarray, it will be restored to a bright Gauss point at a particular location (corresponding to topological charge $-l$) of the far-field OV array, while other locations still hold the ring of OV with a dark center. Therefore, through detecting the bright or dark spots at the center of each OV, we can identify topological charges of incident OVs. In order to verify feasibility of OAM detection using meta-reflectarray, we utility both single OAM and multi-OAMs as incident beam onto the meta-reflectarray. The results are shown in Fig. 4. Figures 4(a)-4(b) demonstrate the single OAM detection with incident topological charge $l = -1$ and $l = -4$, and show gauss point at the position of $l = 1$ in 3×3 OV array and $l = 4$ in 5×5 OV array, respectively. Figures 4(c)-4(d) show the multi-OAMs detection with different topological charges in incident beam.

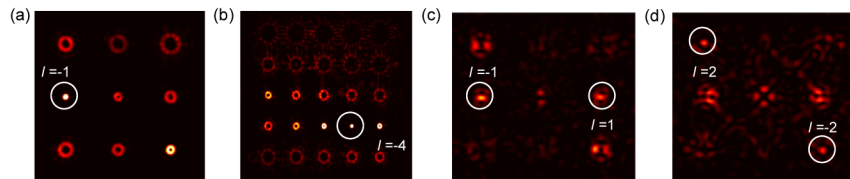


Fig. 4. OAM's detection by meta-reflectarray at 1550nm. (a)-(b) are single OAM detection with $l = -1$ and $l = -4$, respectively. Detectable Gauss point is indicated out with write circle. (c)-(d) are multi-OAMs detection for topological charges $l = \pm 1$ and $l = \pm 2$, respectively.

5. Conclusion

In summary, we theoretically demonstrated a novel method of generation and detection of multi-channel OAM by a micrometer-scale dielectric meta-reflectarray. Different from traditional methods of OAM's generation and detection, our designed meta-reflectarray has the superiorities of miniaturized size, broadband working wavelength, high diffraction efficiency, and generation and detection for multiplex OAMs. Further, by adding a gradient phase, we realize separation of orthogonal polarization through tilt reflection angle from 0 to 45 degree in cross-polarization. For these fascinating characteristics, this method has great potenal applications in photonic integrated devices and systems to realize high-capacity and multi-channel OAM communication. As final remarks, besides the meta-reflectarray based on silicon bars studied here, other metasurfaces can also be considered, for example the

metasurface based on gold-bars with circular polarized light can reach 80% diffraction efficiency [31], and the structure parameters of meta-reflectarray can be further optimized for other wavelengths and reflection angles.

Acknowledgments

This work was supported by the National Natural Science Foundation of China under Grant Nos.61138003, 61427819, 61422506, and 61405121; National Key Basic Research Program of China (973) under grant No.2015CB352004; Science and Technology Innovation Commission of Shenzhen under grant Nos.KQCS2015032416183980, KQCS201532416183981, JCYJ20140418091413543, and the start-up funding at Shenzhen University.